



New Heterocyclic Compounds Based on Pyridazinones Scaffold as Efficient Inhibitor of Corrosion of Mild Steel in Acidic Solution 1 M HCl

Fouad El kalai¹ · Tarik Chelfi¹ · Nouredine Benchat¹ · Mohammed Bouklah¹ · Said Daoui¹ · Khalid Karrouchi² · Mustapha Allali³ · Mustapha Taleb⁴ · Elhachmia Ech-chihbi⁴ · Faisal A. Almalki⁵ · Taibi Ben Hadda^{1,5}

Received: 12 January 2020 / Revised: 1 June 2020 / Accepted: 17 June 2020 / Published online: 24 June 2020
© Springer Nature Switzerland AG 2020

Abstract

The present study deals with the synthesis and the corrosion inhibition performance of three pyridazinone derivatives, namely (E)-6-(4-chlorostyryl)-4-(4-(trifluoromethyl)-benzyl)pyridazin-3(2H)-one (**3a**), (E)-4-(3-chlorobenzyl)-6-(3-chlorostyryl)pyridazin-3(2H)-one (**3b**), and (E)-6-(4-chlorostyryl)-4-(4-methylbenzyl)pyridazin-3(2H)-one (**3c**), was investigated for mild steel corrosion in 1 M HCl medium using weight loss measurements, potentiodynamic polarization (PDP), Electrochemical Impedance Spectroscopy (EIS) techniques. PDP curves reveal that all studied compounds are predicted to be mixed inhibitors influencing both cathodic hydrogen evolution and anodic metal dissolution. Further, EIS study shows that the charge transfer resistance increases with the inhibitor concentration, and the adsorption of **3b** obeys the Langmuir isotherm. Quantum chemical calculation was employed also to correlate the molecular structure of pyridazinone derivatives and their experimental inhibition efficiencies. All results show that **3b** exhibits the best inhibitive action at 10^{-3} M, which may be related to a better electron acceptance ability of this molecule.

Keywords Pyridazin-3(2H)-one · Corrosion inhibition · Mild steel · DFT calculation · Langmuir isotherm · Organic inhibitor

Electronic supplementary material The online version of this article (<https://doi.org/10.1007/s40735-020-00384-5>) contains supplementary material, which is available to authorized users.

✉ Tarik Chelfi
tarikchelfi@gmail.com

Fouad El kalai
fouadchim@gmail.com

- ¹ Laboratory of Applied Chemistry & Environment, Faculty of Sciences, University Mohammed the First, MB 524, 60000 Oujda, Morocco
- ² Laboratory of Medicinal Chemistry, Faculty of Medicine and Pharmacy, University, Mohammed, Rabat, Morocco
- ³ Institute of Nursing Professions and Health Techniques Fez, EL Ghassani Hospital, 30000 Fez, Morocco
- ⁴ Laboratory of Engineering, Electrochemistry, Modeling and Environment (LIEME), Faculty of Sciences, University Sidi Mohamed Ben Abdellah, Fez, Morocco
- ⁵ Department of Pharmaceutical Chemistry, Faculty of Pharmacy, Umm Al-Qura University, Makkah Almukarramah 21955, Saudi Arabia

1 Introduction

Pyridazinones derivatives are very important heterocyclic structures due, on the one hand, to their ease of access through a variety of chemical reactions [1–4], and on the other hand, to their presence in a wide range of biologically active compounds [5–7], such as in agrochemistry, like herbicide compounds [8], fungicides and insecticides [9]. In addition, pyridazinone scaffold show some interesting physicochemical properties, hence their use as good metal extractants from aqueous solutions [10, 11] or as corrosion inhibitors for mild steel was well documented in the last decade [5, 12–16].

Mild steel is very useful in industrial implications because of its exquisite mechanical properties, easy availability, and cost-effectiveness [17]. But, despite its wide application, it is easily affected in aggressive solutions such as hydrochloric acid which is frequently employed for many industrial processes such as pickling, cleaning, and descaling [18, 19].

Protection of metal against corrosion using organic compounds is an important industrial and scientific issue and

among the well-known agents are organic inhibitors containing heteroatoms, such as N, O, P, and S [20, 21]. Functional groups involving these heteroatoms and/or π electron systems are also known to enhance inhibitive properties [22].

The mechanism of action of organic compounds in corrosion inhibition is through adsorption on the metal surface, which depends on the size and electron density of the molecule, the number of adsorption active centers, the mode of adsorption and formation of metal complexes [23, 24].

Thus, the structure and electronic characteristics of organic inhibitors play key factors in facilitating their adsorption at the metal surfaces [22–25].

Furthermore, computational calculation such as DFT was used to explain the correlation between the inhibition efficiency of compounds and the parameters of electronic structures [24].

The present work seeks to explore the potentials of three new pyridazinone derivatives: (E)-6-(4-chlorostyryl)-4-(4-(trifluoromethyl)-benzyl)pyridazin-3(2H)-one (**3a**), (E)-4-(3-chlorobenzyl)-6-(3-chlorostyryl)pyridazin-3(2H)-one (**3b**), and (E)-6-(4-chlorostyryl)-4-(4-methylbenzyl)pyridazin-3(2H)-one (**3c**) as corrosion inhibitors of mild steel corrosion in 1 M HCl. Corrosion reaction was monitored using different techniques such as Weight Loss measurement, potentiodynamic polarization (PDP), Electrochemical Impedance Spectroscopy (EIS). Quantum chemical calculations were carried out to correlate molecular and electronic structures of the inhibitors with their inhibitive performances.

2 Experimental Part

2.1 Chemistry

2.1.1 Synthesis of Chalcones 1a-c

In a 100 ml flask containing 20 ml of toluene are mixed (4 mmol, 0.46 g) of Levulinic acid, (3 drops) of morpholine, (9 drops) of glacial acetic acid, and (4 mmol) of suitable aldehyde. The reaction mixture is refluxed for 12 h. After evaporation of the solvent under reduced pressure; the reaction mixture was cooled and washed with a mixture of acetic acid: water (1: 4). In each case, the precipitate formed was filtered and dried to give the compounds 1a-c.

2.1.2 Synthesis of (E)-6-styryl-4,5-dihydropyridazin-3(2H)-one 2a-c

To 0.01 mol of compound 1a-c in 20 ml of ethanol is added (0.5 g 0.01 mol) of hydrazine hydrate. The mixture is refluxed for four hours. After cooling, (E)

-6-styryl-4,5-dihydropyridazin-3(2H)-one (2a-c) precipitates, is filtered and dried.

2.1.3 Synthesis of Pyridazin-3(2H)-ones 3a-c

In a 100 ml flask contains (20 ml) sodium methanoate (prepared from sodium and anhydrous methanol), 0.05 mol of the compound (2a-c) and 0.05 mol of the appropriate aldehydes. The reaction mixture is stirred overnight at room temperature, after dilution with water, acidified with concentrated HCl to acidic pH. The contents were poured into beaker contains ice water, filtered and recrystallized with ethanol.

2.1.4 (E)-6-(4-chlorostyryl)-4-(4-(trifluoromethyl)benzyl)pyridazin-3(2H)-one 3a

Yellow solid, Yield: 62%, Melting point: 187–189 °C.

^1H NMR (300 MHz, CDCl_3 ; TMS) δ (ppm): 8.05 (s, 1H, H12), 7.86 – 6.33 (m, 8H, H-Ar), 6.09– 5.64 (m, 2H, H7 et H8), 5.20 (s, 1H, H11), 3.86 (s, 2H, H16). ^{13}C NMR (75 MHz, CDCl_3 ; TMS) δ (ppm): 167.31, 159.61, 159.23, 155.02, 149.90, 143.69, 140.31, 135.00, 133.94, 133.35, 133.10, 129.12, 44.15. MS: $[\text{M}]^+$: 391.23 m/z and $[\text{M}^+ \text{Na}]^+$: 413.30 m/z.

2.1.5 (E)-4-(3-chlorobenzyl)-6-(3-chlorostyryl)pyridazin-3(2H)-one 3b

Off-white Solid, Yield: 59%, Melting Point: 180–182 °C.

^1H NMR (500 MHz, $\text{DMSO}-d_6$; TMS) δ (ppm): 13 (s, 1H, H13), 7.97–6.88 (m, 9H, H10 et H-Ar), 6.42 (d, $J=16.4$ Hz, 1H, H7), 5.60 (d, $J=16.5$ Hz, 1H, H8), 3.45 (s, 2H, H16). ^{13}C NMR (126 MHz, $\text{DMSO}-d_6$; TMS) δ (ppm): 141.70, 138.41, 133.40, 133.12, 131.52, 77.23, 76.97, 76.71, 38.68, 38.51, 38.35, 38.18, 38.01, 37.85, 37.68, 31.34, 27.58. MS: $[\text{M}]^+$: 357.21.

2.1.6 (E)-6-(4-chlorostyryl)-4-(4-methylbenzyl)pyridazin-3(2H)-one 3c

Yellow Solid, Yield: 52%, melting point: 190–192 °C. ^1H NMR (500 MHz, $\text{DMSO}-d_6$; TMS) δ (ppm): 13.01 (s, 1H, H13), 7.73–7.19 (m, 8H, H-Ar), 7.10 (d, $J=7.6$ Hz, 2H, H8 et H10), 7.05 (d, $J=16.6$ Hz, 1H, H7), 3.76 (s, 2H, H17), 2.25 (s, 3H, H24). ^{13}C NMR (126 MHz, $\text{DMSO}-d_6$; TMS) δ (ppm): 161.64, 143.49, 140.94, 135.22, 135.13, 132.50, 34.66. MS: $[\text{M}]^+$: 337.12 m/z.

3 Materials and Reagents

Mild steel coupons with the following chemical composition: 0.17 wt.% C, 0.37 wt.% Mn, 0.20 wt.% Si, 0.03 wt.% S, 0.01 wt.% P and balance Fe). For the gravimetric and electrochemical measurements, pre-treatment of the surface of specimens was carried out by polished with emery paper at different grit sizes (from 180 to 2000), cleaned with distilled water, degreasing in acetone, and dried before use.

The aggressive medium (1 M HCl) was prepared by dilution of analytical-grade 37% HCl with distilled water. The concentration range of pyridazine derivatives was varied from 10^{-6} M to 10^{-3} M and the blank solution was also prepared for comparison.

3.1 Weight Loss Measurements

The steel specimens were weighed accurately and immersed in 50 mL solution without and with different inhibitors concentrations in 1 M HCl solution at 298 K for 6 h of immersion.

The temperature of the electrolyte solution was maintained at 298 K in a thermostat-controlled water bath. After immersion, the specimens were taken out, washed, dried, and reweighed accurately. The values calculated of W_{corr} and inhibition efficiency is defined as follows [26, 27]:

$$W_{\text{corr}} = \frac{m_i - m_f}{S \cdot t} \quad (1)$$

$$\eta_w = \frac{W_{\text{corr}} - W'_{\text{corr}}}{W_{\text{corr}}} \times 100 \quad (2)$$

where m_i and m_f are the mass of the specimens before and after immersion to the test solutions, S is the exposed surface area of the steel specimens (cm^2), t is the exposure time (h), W_{corr} and W'_{corr} are the corrosion rate of carbon steel in the absence and presence of inhibitor, respectively.

3.2 Electrochemical Measurements

EIS and potentiodynamic polarization measurements were carried out in a conventional three-electrode cell using Voltalab PGZ100, Radiometer Analytical piloted by VoltMaster4 software [28]. A three-electrode electrochemical setup comprising the platinum counter electrode (CE), Ag/AgCl reference electrode (RE), and mild steel working electrode (WE). The polarization curves were plotted by changing the electrode potential from -900 mV/ E_{corr} to 100 mV/ E_{corr} with a slow scan rate (1 mV/s). The working electrode was immersed in a test solution for 30 min to establish a steady-state open circuit potential (E_{ocp}). The corrosion $\eta_{\text{pp}}\%$

was calculated from the corrosion current density by the following formula (3):

$$\eta_{\text{pp}}\% = \frac{i_{\text{corr}} - i'_{\text{corr}}}{i_{\text{corr}}} \times 100 \quad (3)$$

EIS measurements were performed at open circuit potential with an amplitude 10 mV peak to peak in the frequency range of 100 kHz to 10 mHz. The charge transfer resistance was calculated from the Nyquist plot from which efficiency has been calculated using the Eq. (4).

$$\eta_{\text{imp}}\% = \frac{R_{\text{ct}} - R'_{\text{ct}}}{R_{\text{ct}}} \times 100 \quad (4)$$

where, R'_{ct} and R_{ct} are the charge transfer resistance in the absence and presence of the inhibitor, respectively.

3.3 Quantum Chemical Calculations

All the quantum chemical calculations were performed for studied molecules to carry out the complete optimized geometry using Gaussian 09 software [29, 30]. The molecular structures of the studied compounds were fully optimized by using density functional theory method DFT-B3LYP with the 6-31G (d,p) basis set in the gas phase.

The quantum chemical descriptors such as energy gap $\Delta E(E_{\text{HOMO}} - E_{\text{LUMO}})$, η (global hardness), σ (softness), μ (dipole moment), χ (electronegativity) and ΔN which represent the fraction of electrons transferred from the inhibitor molecule to the metal surface were calculated using E_{HOMO} (the highest occupied molecular orbital energy) and E_{LUMO} (the lowest unoccupied molecular orbital energy) and the following Eqs. 5–9 [12, 30]:

$$\eta = \frac{(E_{\text{LUMO}} - E_{\text{HOMO}})}{2} \quad (5)$$

$$\sigma = \frac{1}{\eta} \quad (6)$$

$$\chi = \frac{-(E_{\text{HOMO}} + E_{\text{LUMO}})}{2} \quad (7)$$

$$\omega = \frac{\chi^2}{2\eta} \quad (8)$$

$$\Delta N = \frac{\chi_{\text{Fe}} - \chi_{\text{inh}}}{[2(\eta_{\text{Fe}} + \eta_{\text{inh}})]} \quad (9)$$

where: χ_{Fe} and χ_{inh} : Are the absolute electronegativity of metal and inhibitor molecules respectively. η_{Fe} and η_{inh} : Are

the absolute hardness of metal and the inhibitor molecule, respectively.

Using a theoretical value of $\chi_{\text{Fe}} = 7.0$ eV and $\eta_{\text{Fe}} = 0$ for the computation of the fraction of transferred electrons.

4 Results and Discussion

4.1 Synthesis of Functionalized Pyridazinones

In the aim to have access to new functionalized pyridazinones **3a-c**, a three-step procedure has been used. Initially, a condensation step between Levulinic acid and aromatic aldehyde leads to the formation of chalcones **1a-c**, which, secondly, in the presence of hydrazine hydrate in ethanol produce dihydropyridazinones **2a-c**. Finally, the action of the appropriate aromatic aldehyde leads to the formation of the corresponding pyridazinones **3a-c** characterized with the help of different spectral techniques such as ^1H NMR, ^{13}C NMR, and Mass spectrometry. (Scheme 1).

4.2 Weight Loss Measurements (WL)

The corrosion rate and inhibition efficiencies obtained from the Weight Loss experiments in the presence of different concentrations of inhibitors in 1 M HCl are listed in Table 1.

The results showed that the inhibition performance of all the studied inhibitors increases with concentration and displays a maximum inhibition efficiency of 71.9% for **3a**, 86.1% for **3b**, and 62.3% for **3c** at 10^{-3} M. Thus, all studied compounds were proven to be good efficient corrosion inhibitors for mild steel. The trend of corrosion inhibition efficiency was found as $3b > 3a > 3c$.

This good anti-corrosion performance of these compounds was due to the presence of π -bonds in aromatic moieties, the lone pair electron of heteroatoms (N and O)

Table 1 Corrosion rate W_{corr} values and inhibition efficiency η_w (%) of mild steel in 1 M HCl obtained from gravimetric measurements at 298 K

| Medium | Concentration (M) | W_{corr} (mg/cm ² .h) | η_w % |
|---------|-------------------|---|------------|
| 1 M HCl | — | 0.689 | — |
| 3a | 10^{-6} | 0.496 | 28.0 |
| | 10^{-5} | 0.425 | 38.2 |
| | 10^{-4} | 0.391 | 43.2 |
| | 10^{-3} | 0.193 | 71.9 |
| 3b | 10^{-6} | 0.263 | 61.7 |
| | 10^{-5} | 0.259 | 62.3 |
| | 10^{-4} | 0.195 | 71.6 |
| | 10^{-3} | 0.095 | 86.1 |
| 3c | 10^{-6} | 0.553 | 19.6 |
| | 10^{-5} | 0.425 | 38.2 |
| | 10^{-4} | 0.355 | 48.3 |
| | 10^{-3} | 0.259 | 62.3 |

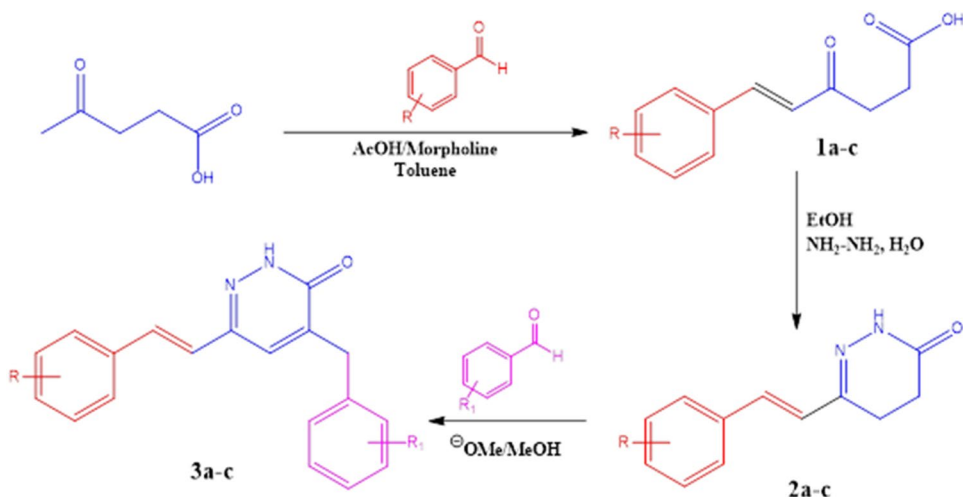
as well as the polar functional groups which promote the complexation with Fe.

4.3 Electrochemical Measurements

4.3.1 Potentiodynamic Polarization (PDP)

Potentiodynamic polarization experiments have been performed for Pyridazinones derivatives with their varied concentrations in 1 M HCl to extract information related to the kinetics of corrosion inhibition phenomenon. Figure 1. shows representative Tafel polarization plots of mild steel in 1 M HCl solution in the absence and presence of various concentrations of tested compounds at 25 ± 2 °C. Polarization studies show that the corrosion current density decreases by increasing the concentration of inhibitors.

Scheme 1 Synthesis of functionalized pyridazinones **3a-c**



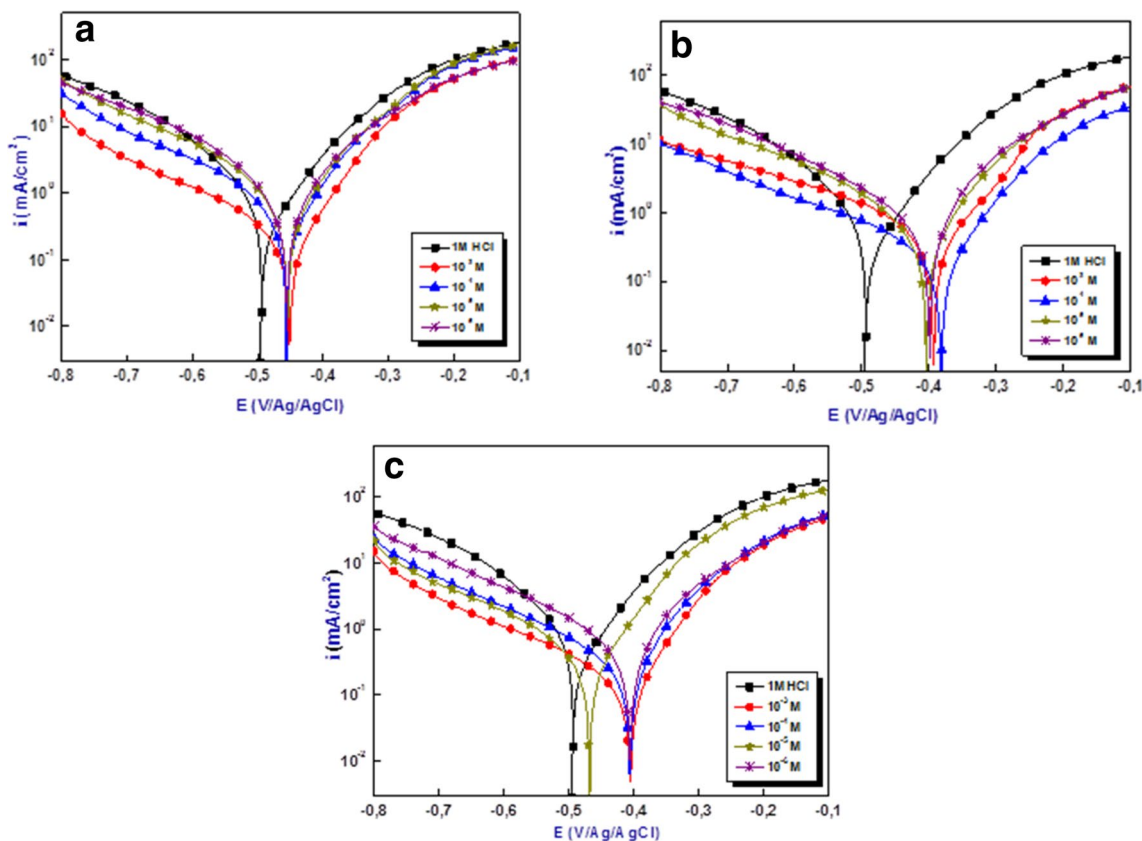


Fig. 1 Tafel polarization curves for mild steel obtained at 298 K in 1 M HCl solution containing different concentrations of tested compounds

This indicates that these molecules act as corrosion inhibitors suppressing both anodic and cathodic reactions by getting adsorbed onto the steel surface as they simply block the active sites.

Electrochemical parameters related to the kinetics of the corrosion process were derived from extrapolation of the linear Tafel regions to the corrosion potential and the results are listed in Table 2. From this table, it can be noticed that the corrosion current density values (i_{corr}) decrease in the presence of the inhibitors. Generally, a compound can be classified as an anodic or a cathodic type inhibitor based on the shift of the E_{corr} values. If the displacement is > 85 mV concerning E_{corr} of the blank (1 M HCl), the inhibitor acts either as a cathodic or an anodic type. Otherwise, it is treated as mixed-type [23]. In the present study, the maximum displacements for **3a** and **3b** are less than 85 mV, indicating that these compounds act as mixed-type inhibitors affecting both anodic oxidative metallic dissolution as well as cathodic reductive evolution of hydrogen reactions. However, **3c** is an anodic-type inhibitor (displacement up to 85 mV). Also, a slight change occurs in β_c values with increasing the concentration of the Pyridazinones derivatives i.e. their values are almost constant [31]. These results can be explained by the adsorption of **3a**, **3ab**, and **3c** over the mild steel surface and

Table 2 Polarization parameters and corresponding inhibition efficiency for the mild steel obtained at 298 K in 1 M HCl solution with and without the addition of different concentrations of **3a**, **3b**, and **3c**

| Medium | Conc. M | $-E_{corr}$ mV/Ag/ AgCl | i_{corr} $\mu A\ cm^{-2}$ | $-\beta_c$ mV dec ⁻¹ | η_{pp} % |
|-----------|-----------|-------------------------------|-----------------------------|------------------------------------|---------------|
| 1 M HCl | – | 498 | 983 | 150 | – |
| 3a | 10^{-6} | 456 | 882 | 128 | 10,3 |
| | 10^{-5} | 454 | 812 | 137 | 17,4 |
| | 10^{-4} | 457 | 598 | 130 | 39,1 |
| | 10^{-3} | 451 | 303 | 144 | 69,1 |
| 3b | 10^{-6} | 449 | 414 | 129 | 57,9 |
| | 10^{-5} | 461 | 406 | 133 | 58,7 |
| | 10^{-4} | 462 | 314 | 135 | 68,0 |
| | 10^{-3} | 452 | 155 | 138 | 84,2 |
| 3c | 10^{-6} | 407 | 821 | 132 | 16,4 |
| | 10^{-5} | 467 | 542 | 137 | 44,8 |
| | 10^{-4} | 407 | 469 | 140 | 52,2 |
| | 10^{-3} | 405 | 373 | 139 | 62,0 |

slow down the corrosion process by just overcrowding the reaction sites which are present over the mild steel surface without changing the mechanism of metal dissolution. These

results are in good accordance with the results obtained from weight loss measurements.

4.3.2 Electrochemical Impedance Spectroscopy (EIS)

To improve the results extracted from weight loss and potentiodynamic polarization results, EIS spectra presented as Nyquist plots recorded for mild steel after ½ h immersion in 1 M HCl solution in the absence and presence of different concentrations of investigated compounds are shown in Fig. 2. Nyquist plots exhibit a depressed semicircle. This is often due to frequency dispersion as a result of the roughness and inhomogeneity of the electrode surface [32]. This result implies that the corrosion of mild steel in 1 M HCl solution is mainly controlled by the charge transfer process [33, 34].

It can also be seen that the diameter of the Nyquist semicircle increases with increasing concentration of studied compounds over the entire concentration range, indicating the formation of the protective film on the metal surface. CPE/ndI is used instead of the capacitor to consider the non-idealities coming from the inhomogeneity of the electrode

surface [35]. The CPE is defined in impedance representation as:

$$Z_{CPE} = [Q(j\omega)^n]^{-1} \quad (10)$$

where Q represents the CPE constant, ω is the angular frequency; j represents the imaginary number and n is an exponent related to the phase shift and can be used as a measure of surface inhomogeneity.

EIS data are simulated by the proposed equivalent circuit presented in Fig. 3 where R_s is the solution resistance, R_{ct} denotes the charge-transfer resistance, and CPE is the constant phase element.

The impedance parameter values of R_s ($\Omega \text{ cm}^2$), R_{ct} ($\Omega \text{ cm}^2$), C_{dl} ($\mu\text{F cm}^{-2}$), Q ($\mu\text{F.Sn}^{-1}$), n_{dl} and η_{imp} (%) are summarized in Table 3. It could be noted from Table 3 that the R_{ct} values increase and the C_{dl} values tend to decrease with the concentration of the studied compounds. This is attributed to the increase in the surface coverage by the inhibitors leading to an increased inhibition efficiency. The variation in R_{ct} and C_{dl} is explained by the gradual replacement of water molecules by the composites on the

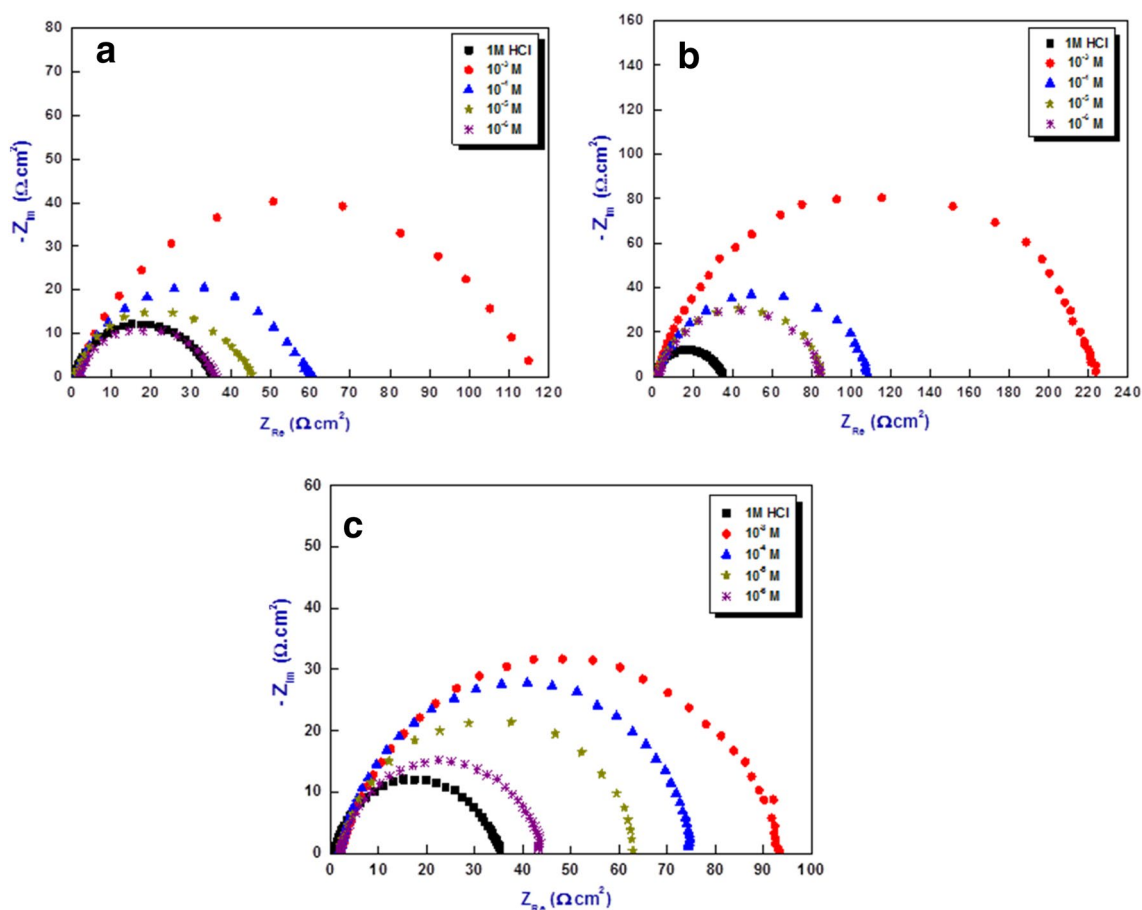


Fig.2 Nyquist impedance diagrams for mild steel obtained at 298 K in 1 M HCl solution containing different concentrations of title compounds

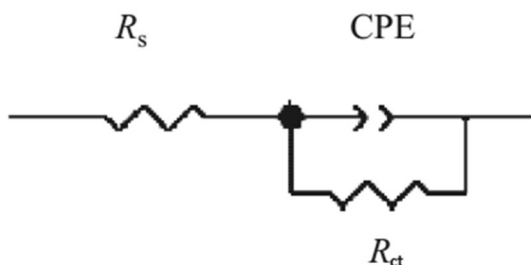


Fig. 3 Electrical equivalent circuit used for the modeling mild steel/HCl 1 M

mild steel surface [29]. The slight deviation of the value of n_{dl} from unity can be related to the deviation of CPE from the ideal capacitive behavior due to inhomogeneity on the metal surface [36],[37]. The highest value of R_p (218.0 Ω cm^2) and the lowest value of C_{dl} (31.7 μF cm^{-2}) have been found for **3b** at an optimum concentration (10⁻³ M). This result shows that the inhibitive performance of **3b** is better than that **3a** and **3c**.

The inhibition efficiencies η_{imp} of mild steel in the presence of a high concentration of inhibitors follow the sequence: **3b** > **3a** > **3c**. The strong adsorption of these compounds can be explained by the presence of heteroatoms (O and N), halogen atoms as well as π -electrons of the aromatic rings. The replacement of hydrogen atoms in **3c** by fluorine atoms in **3a** increases its inhibition ability. This can be explained by the larger area coverage created by this compound during their adsorption onto the steel surface. The obtained results are in good agreement with those obtained from PDP and WL measurements.

4.3.3 Adsorption Isotherm and Thermodynamic Parameters

The corrosion inhibition process is based on the adsorption of the inhibitors onto the metal surface. The selection of an efficient anti-corrosion compound is mainly dependent on its adsorption ability onto the metal surface [38]. Fundamental information on the interaction between the inhibitors and the mild steel surface is given by the adsorption isotherms. The value of the linear regression coefficient (R^2) was used as a gauge in selecting the isotherm that best described the adsorption process onto the metal surface [29]. Langmuir isotherm is the first sorption model that we will consider. It is described by the equation [30].

$$\frac{C_{inh}}{\theta} = C_{inh} + \frac{1}{K} \tag{11}$$

where C_{inh} is the concentration of the inhibitor, θ is the surface coverage of the inhibitor; and K is the equilibrium constant of the adsorption/desorption process.

This model assumes that the solid surface contains a fixed number of adsorption sites and each site holds one adsorbed species [39].

The best description of the adsorption behavior of the studied inhibitors was explained by Langmuir adsorption isotherm (Fig. 4) as the average linear regression coefficient values (R^2) and slope are very close to 1. The linear relationships of C_{inh}/θ versus C_{inh} are illustrated in Fig. 2. The deviation from 1 can be explained by the interaction between the adsorbed species on the steel surface and/or to the non-homogeneous surface of the metal [40].

The Gibbs-free energy change of adsorption (ΔG_{ads}) can be calculated by the following equation [41] and presented in Table 4:

Table 3 Electrochemical parameters of impedance and corresponding inhibition efficiency for the mild steel obtained at 298 K in 1 M HCl solution with and without the addition of different concentrations of **3a**, **3b**, and **3c**

| Medium | Conc (M) | R_s (Ω cm^2) | R_{ct} (Ω cm^2) | C_{dl} (μF cm^{-2}) | n_{dl} | Q (μF S n^{-1}) | Θ | η_{imp} % |
|---------|------------------|---------------------------|------------------------------|--------------------------------|----------|------------------------------|----------|----------------|
| 1 M HCl | – | 1.1 | 35.0 | 121.0 | 0.773 | 419.0 | – | – |
| 3a | 10 ⁻⁶ | 1.8 | 38.8 | 95.1 | 0.769 | 356.0 | 0.097 | 9,7 |
| | 10 ⁻⁵ | 1.2 | 42.2 | 91.1 | 0.830 | 234.1 | 0.170 | 17,0 |
| | 10 ⁻⁴ | 1.3 | 57.2 | 64.2 | 0.823 | 137.3 | 0.388 | 38,8 |
| | 10 ⁻³ | 1.8 | 110.9 | 49.6 | 0.816 | 128.7 | 0.684 | 68,4 |
| 3b | 10 ⁻⁶ | 2.5 | 82.5 | 89.0 | 0.812 | 223.6 | 0.575 | 57,5 |
| | 10 ⁻⁵ | 1.6 | 84.2 | 55.7 | 0.814 | 150.7 | 0.584 | 58,4 |
| | 10 ⁻⁴ | 1.9 | 107.6 | 50.3 | 0.801 | 141.9 | 0.674 | 67,4 |
| | 10 ⁻³ | 2.3 | 218.0 | 31.7 | 0.860 | 63.5 | 0.839 | 83,9 |
| 3c | 10 ⁻⁶ | 1.8 | 41.8 | 77.5 | 0.806 | 234.9 | 0.162 | 16,2 |
| | 10 ⁻⁵ | 1.5 | 62.9 | 76.4 | 0.793 | 187.9 | 0.443 | 44,3 |
| | 10 ⁻⁴ | 1.7 | 72.9 | 75.8 | 0.835 | 178.3 | 0.519 | 51,9 |
| | 10 ⁻³ | 2.0 | 90.8 | 52.5 | 0.798 | 154.1 | 0.614 | 61,4 |

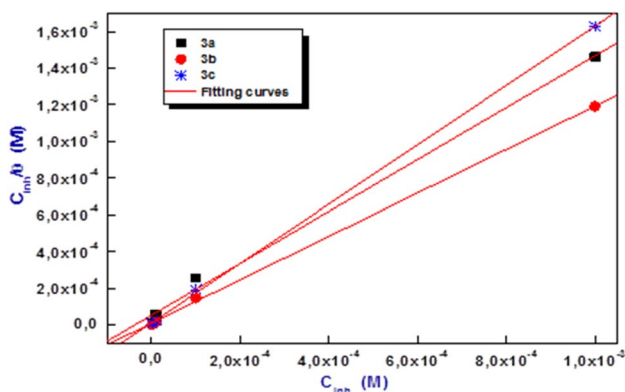


Fig. 4 Langmuir adsorption isotherm for mild steel in 1 M HCl solution containing various concentrations of **3a**, **3b**, and **3c** at 298 K

Table 4 Thermodynamic parameters for the adsorption of inhibitors on mild steel at 298 K

| Inhibitor | K (L/mol) | ΔG_{ads} (Kj/mol) | R ² |
|-----------|----------------------|---------------------------|----------------|
| 3a | 18.3 10 ³ | -34.3 | 0.99785 |
| 3b | 87.7 10 ³ | -38.1 | 0.99974 |
| 3c | 74.5 10 ³ | -37.7 | 0.99988 |

$$\Delta G_{ads} = RT \ln 55.5K \tag{12}$$

where *R* is the gas constant, *T* is the absolute temperature and 55.5 is the concentration of water in solution in M⁻¹.

Generally, high values of *K* allow more adsorption [42]. The high values of *K* is an indication that these compounds adsorbed strongly on the mild steel surface. It is well known also that ΔG_{ads} values of up to -20 kJ/mol indicate adsorption with electrostatic interaction between the adsorbent and adsorbate (physisorption), while negative values of more than -40 kJ/mol involve the sharing or transfer of electrons from organic molecules to the metal surface to form a coordinate type of bond (chemisorption) [43]. The value of ΔG_{ads} in the present study suggests that the adsorption of molecules of P2 may involve both physisorption and chemisorption mechanisms.

4.3.4 Effect of Temperature and Thermodynamics Parameters

Temperature variation causes an effective change in the inhibition activity of inhibitors. Therefore, the inhibition effect of the investigated compounds was studied at a concentration of 10⁻³ M and temperature ranging from 298 to 328 K, using the potentiodynamic polarization technique. The Tafel curves obtained are presented in Fig. 5.

According to Fig. 5, there is a clear acceleration of the cathodic and anodic reactions with increasing the

temperature. The corresponding parameters (*E_{corr}*, *i_{corr}*, *b_c*, and η_{pp}) obtained from Tafel curves are given in Table 5. Table 5 shows that *i_{corr}* values decrease as the temperature increases from 298 to 328 K, this is due to an appreciable decrease in the adsorption of inhibitor molecules onto the metal surface due to a reduction in stability of the adsorbed film at higher temperatures. Besides, the corrosion current density of mild steel increased more rapidly with temperature increases in the absence of studied molecules. These results confirmed that the **3a**, **3b**, and **3c** compounds acted as efficient corrosion inhibitors in all the range of the temperatures studied.

The activation parameters have an important role in understanding the inhibition mechanism of inhibitors. The dependence of activation energy on temperature for the corrosion process is calculated from the Arrhenius Eq. (13) [44]:

$$i_{corr} = Ae^{\frac{-E_a}{RT}} \tag{13}$$

where *E_a* is the apparent activation energy, *T* is the absolute temperature, *A* is the Arrhenius pre-exponential constant, and *R* is the gas constant.

The activation energy (*E_a*) values in the absence and presence of pyridazinone derivatives were calculated using the logarithm of the Arrhenius Eq. (13). The plots of $\ln i_{corr}$ versus 1000/*T* with and without inhibitor at different concentrations gave straight lines (Fig. 6). The values of the standard enthalpy of activation (ΔH_a) and standard entropy of activation (ΔS_a) for the dissolution of MS were calculated using the following equation [45].

$$\ln\left(\frac{i_{corr}}{T}\right) = \left[\ln\left(\frac{R}{hN_a}\right) + \left(\frac{\Delta S_a}{R}\right) \right] - \frac{\Delta H_a}{RT} \tag{14}$$

where *i_{corr}* is the corrosion current density, *A* is the pre-exponential factor, *h* is Planck’s constant, *N_a* is Avogadro’s number, *E_a* is the apparent activation energy, *R* is the gas constant (*R* = 8.314 J.mol⁻¹.K⁻¹) and *T* is the absolute temperature. The plots of $\log(i_{corr}/T)$ versus 1/*T* gave straight lines (Fig. 6) with slope values equal to ($\Delta H_a/2.303R$) and intercepts of [$\ln(R/hN_a) + (\Delta S_a/2.303R)$]. The calculated values of ΔH_a and ΔS_a in the absence and presence of 10⁻³ M of **3a**, **3b**, and **3c** are listed in Table 6.

Generally, the lower activation energy values of the corrosion process in the presence of the inhibitors are attributed to their chemisorption, while the opposite is generally attributed to their physical adsorption [46]. The obtained values of *E_a* in solutions containing the inhibitors are higher than those in the blank solution. These higher values of apparent activation energy suggest that all inhibitors could be physisorbed onto the mild steel surface. The positive values of ΔH_a reflect the endothermic nature of the mild steel dissolution process [47, 48]. Moreover,

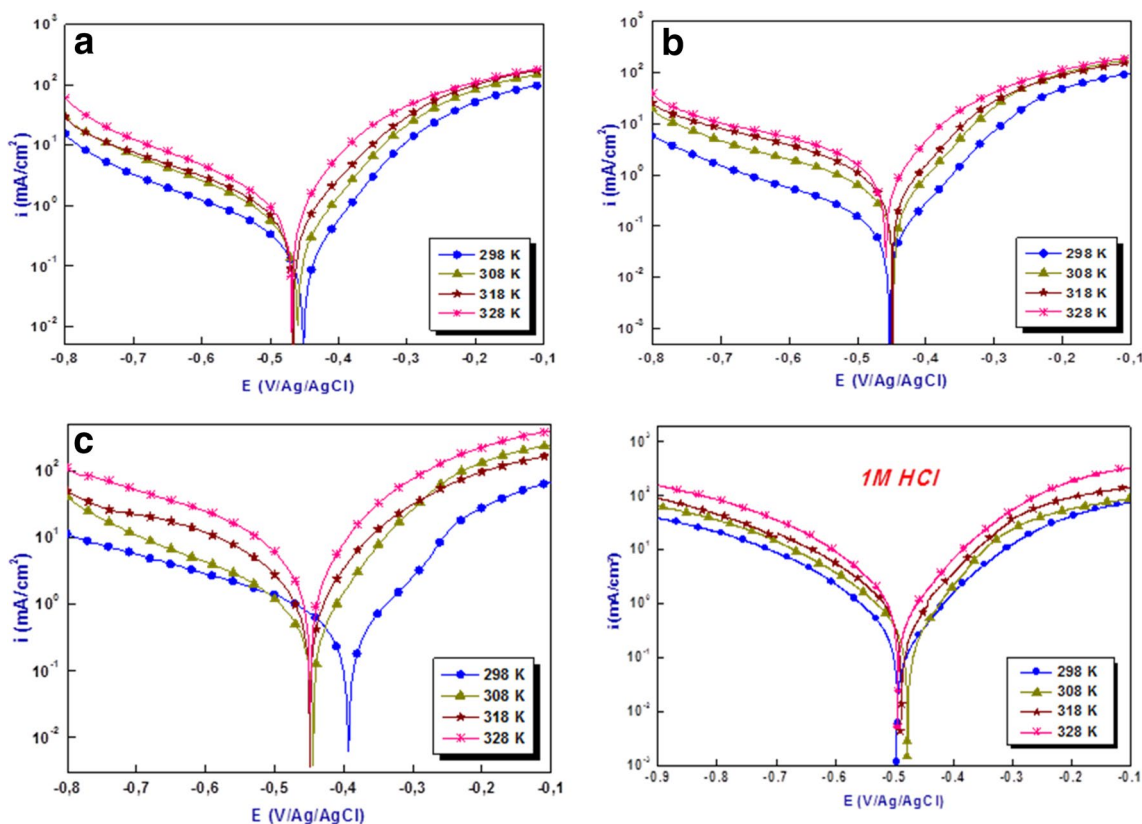


Fig. 5 Potentiodynamic polarization curves for mild steel immersed in 1 M HCl at various temperatures (298–328 K)

Table 5 Polarization parameters and corresponding inhibition efficiencies for tested compounds in 1 M HCl solution at different temperatures

| Medium | Temperature K | $-E_{corr}$ mV/Ag/AgCl | i_{corr} $\mu\text{A}\cdot\text{cm}^{-2}$ | $-\beta_c$ mV.dec $^{-1}$ | β_a mV.dec $^{-1}$ | η_{PP} % |
|---------|---------------|------------------------|---|---------------------------|--------------------------|---------------|
| 1 M HCl | 298 | 498 | 983 | 140 | 150 | – |
| | 308 | 477 | 1200 | 184 | 112 | – |
| | 318 | 487 | 1450 | 171 | 124 | – |
| | 328 | 493 | 2200 | 161 | 118 | – |
| 3a | 298 | 451 | 303 | 144 | 132 | 69.1 |
| | 308 | 459 | 397 | 149 | 118 | 66.9 |
| | 318 | 466 | 514 | 154 | 129 | 64.5 |
| | 328 | 469 | 834 | 157 | 118 | 62.1 |
| 3b | 298 | 452 | 155 | 138 | 135 | 84.2 |
| | 308 | 447 | 216 | 149 | 116 | 82.0 |
| | 318 | 448 | 298 | 164 | 126 | 79.4 |
| | 328 | 458 | 509 | 160 | 123 | 76.8 |
| 3c | 298 | 405 | 373 | 139 | 130 | 62.0 |
| | 308 | 468 | 484 | 148 | 117 | 59.6 |
| | 318 | 462 | 622 | 156 | 126 | 57.1 |
| | 328 | 469 | 997 | 165 | 120 | 54.6 |

the entropy of activation increases in the presence of the studied inhibitors compared to the free acid solution. This increase implies that the Fe-inhibitor complex is less ordered.

4.3.5 Quantum Chemical Calculation

Quantum chemical calculations were employed to give important information about the reactivity and stabilities

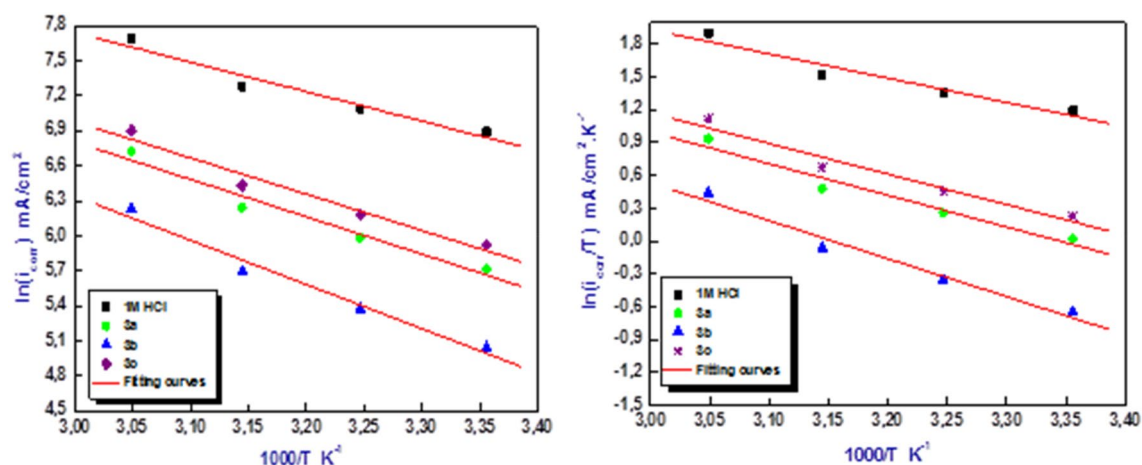


Fig. 6 Arrhenius plots for mild steel corrosion in 1 M HCl in the absence and presence of 10^3 M of pyridazinones **3a-c**

Table 6 Thermodynamic activation parameters of mild steel for studied inhibitors in 1 M HCl solutions obtained from potentiodynamic measurements

| Medium | E_a (KJ.mol ⁻¹) | ΔH_a (KJ.mol ⁻¹) | ΔS_a (KJ.mol ⁻¹ .K ⁻¹) |
|---------|-------------------------------|--------------------------------------|---|
| 1 M HCl | 21.0 | 18.5 | -126.0 |
| 3a | 26.6 | 24.0 | -117.0 |
| 3b | 31.5 | 28.8 | -106.4 |
| 3c | 25.8 | 23.3 | -117.9 |

of the molecules. Quantum chemical parameters for neutral forms of studied molecules in gas phases such as the energy of the highest occupied molecular orbital (HOMO), the energy of the lowest unoccupied molecular orbital (LUMO), energy gap (ΔE_{gap}), dipole moment (μ), electronegativity (χ), hardness (η), softness (σ), fraction of transferred electrons (ΔN) and total energy (T.E) were calculated and given in Table 7.

Quantum chemical parameters, such as E_{HOMO} , are often associated with the electron-donating ability of the molecule [49, 50]. Higher HOMO energy level means that the molecule easily provides electrons to the unoccupied orbital of the metal atoms [51]. Therefore, the binding ability of the inhibitor to the metal surface increases with increasing HOMO and decreasing LUMO energy values. From Table 2,

it can be seen that **3b** has the highest E_{HOMO} value indicating the highest tendency to donate electrons to an electron-deficient site and the lowest value of E_{LUMO} indicating the highest tendency to accept electrons. These results imply that **3b** has the highest tendency to adsorb onto the mild steel surface and this agrees with its highest inhibition efficiency observed in the experiments.

The energy gap (ΔE_{gap}) is also an important parameter that indicates the adsorption ability of the inhibitor onto the metal surface [26]. It should be stated that a good corrosion inhibitor is qualified by a small energy gap because a molecule having a small energy gap is softer than others and can give electrons more readily to metals [52]. Table 7 shows that **3b** has the smallest energy gap value (3.103 eV) compared to **3a** (3.707 eV) and **3c** (3.727 eV), which explains the highest ability of **3b** to adsorb onto the metal surface and form coordinate bonds with the d -orbitals of the steel.

The position of the Cl atoms influences the inhibitory power of the compound. These functional atoms tend to form strong bonds with the metal.

The dipole moment is a measure of the polarity which is related to the distribution of electrons in molecular structure and is also a good indicator of reactivity [53]. The values of μ follow the order of **3b** > **3a** > **3c**, which shows the higher adsorption ability of molecule **3b**.

The softness (σ) is a measure of the polarizability of the molecule and it should be noted that the softer the molecule,

Table 7 Selected quantum chemical parameters for the studied pyridazinones

| Inhibitors | T.E (eV) | E_{HOMO} (eV) | E_{LUMO} (eV) | ΔE (eV) | η (eV) | σ (eV ⁻¹) | χ (eV) | ΔN | Dipole (Debye) |
|------------|-------------|------------------------|------------------------|-----------------|-------------|------------------------------|-------------|------------|----------------|
| 3a | -46,669.245 | -5.873 | -2.165 | 3.707 | 1.853 | 0.539 | 4.019 | 0.803 | 1.0115 |
| 3b | -32,056.365 | -5.659 | -2.556 | 3.103 | 1.551 | 0.644 | 4.107 | 0.931 | 2.9522 |
| 3c | -38,567.824 | -5.748 | -2.021 | 3.727 | 1.863 | 0.536 | 3.885 | 0.835 | 2.2426 |

the better it acts as corrosion inhibitors. Therefore, the higher value of σ (0.644 eV^{-1}) is related to the high reactivity of **3b**.

The fraction of electron transferred (ΔN) is related to the high inhibitive performance and explain by the simple movement of electrons from the donor to the acceptor of the molecule [54]. According to Lukovits et al. [55], if the value of $\Delta N < 3.6$, the inhibition efficiency increases with increasing electron-donating ability of the inhibitor to the metal surface. The nitrogen, oxygen, and halogen atoms of the inhibitor molecules of pyridazinone derivatives allowed it to be adsorbed readily on the metal surface forming an insoluble stable film on the metal surface thus decreasing metal dissolution.

Figure 7 reports the optimized structures and the frontier molecular orbital density distribution of the pyridazinone molecules. Figure 7 shows that the distribution of HOMO and LUMO of all the studied molecules is

almost similar and is mainly localized in the pyridazinone and phenyl rings; consequently, this is the favorite site for interaction with the metal surface.

Molecular electrostatic potential (MEP) helps to visualize the regions of a molecule containing particularly high or low electron density, thus highlighting the reactive centers of the molecule [56]. The MEP surfaces of both pyridazinone compounds are shown in Fig. 8. The various charged regions are represented by different colors, the red regions being the most electron-rich regions of a molecule, whereas blue regions as being the most positive electrostatic potential [57, 58].

The electrophilic active regions were observed to be localized around the oxygen and nitrogen atoms (especially N7 and N14) in the pyridazinone ring. These correspond to the reactive centers of the studied compounds, i.e., the most likely adsorption sites in the corrosion inhibition process. On the other hand, the most positive

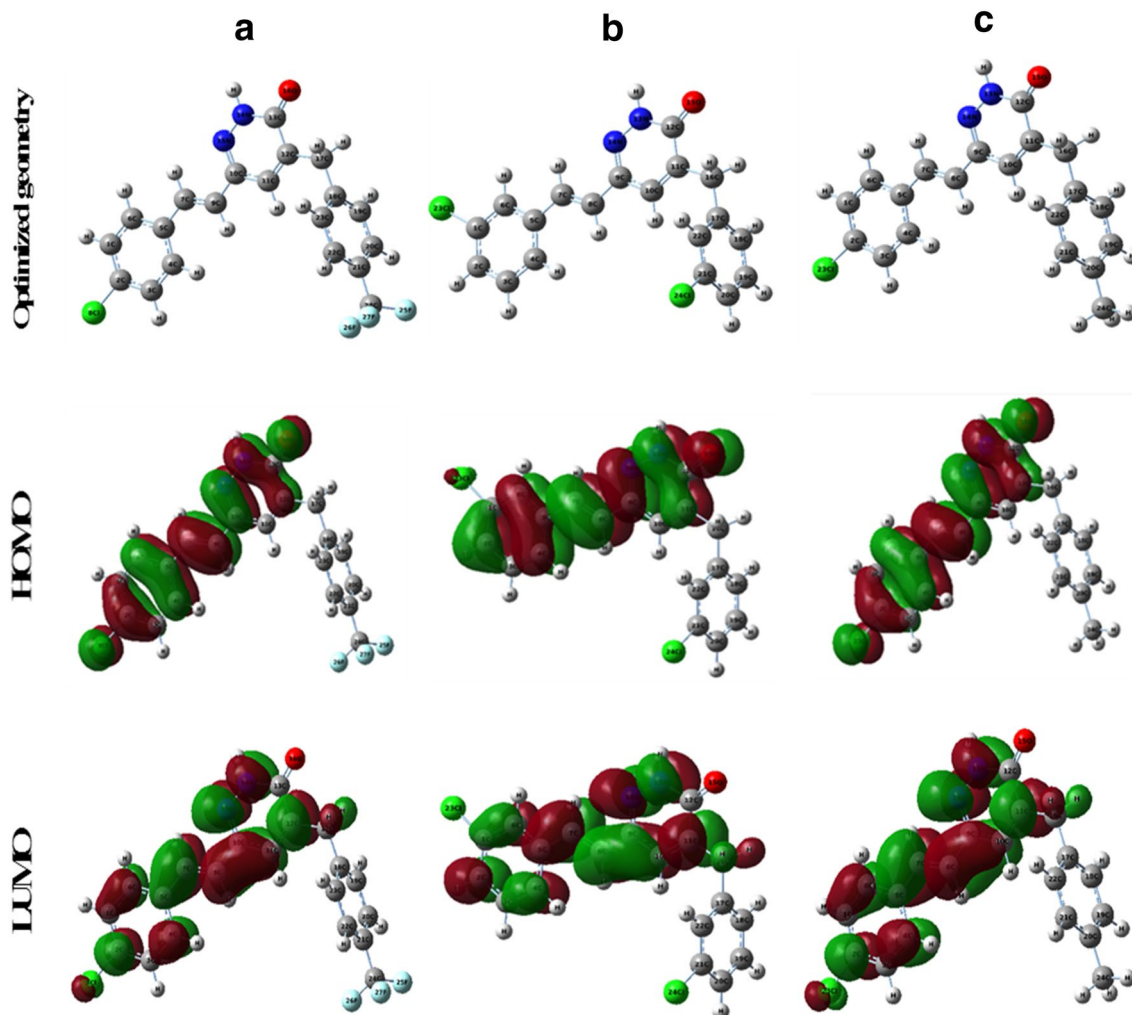


Fig. 7 Optimized structures, HOMO, LUMO, and Molecular electrostatic potential of pyridazinone compounds using DFT/6-31G (d,p) calculation level

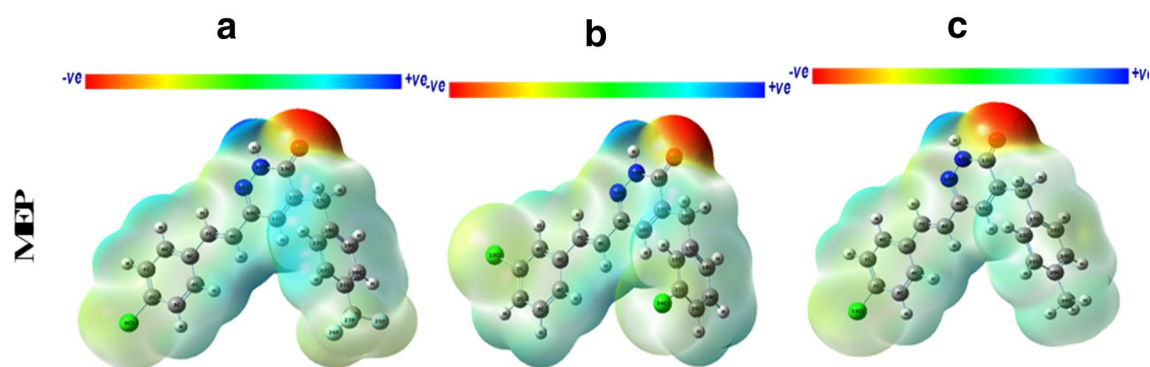


Fig. 8 Molecular electrostatic potential of pyridazinone compounds using DFT/6-31G (d,p) calculation level

electrostatic potential sites are around the hydrogen atoms for both compounds.

5 Conclusions

- The results showed that pyridazinone derivatives **3a**, **3b**, and **3c** show good inhibition properties of the corrosion of mild steel in 1 M HCl, with PYZ2 having the best performance.
- EIS study revealed that the investigated compounds retard corrosion of mild steel through adsorbing onto the metal surface, and the inhibition efficiency increases with an increase in concentration.
- The adsorption of these molecules onto the steel surface has been described by Langmuir adsorption isotherm.
- PDP study showed that all compounds act as mixed-type inhibitors. EIS measurements indicate that with increasing concentrations the charge transfer resistance (R_{ct}) increases, while the double-layer capacitance (C_{dl}) decreases.
- The thermodynamic parameters of adsorption suggest the spontaneity and physical nature of the process.
- Both experimental and quantum chemical calculation results showed that the inhibition efficiency of the inhibitor **3b** is higher than that of **3a** and **3c**.

Compliance with Ethical Standards

Conflict of interest The authors declare that they have no known competing for financial interests or personal relationships that could have appeared to influence the work reported in this paper.

References

1. Hovakimyan SA, Babakhanyan AV, Voskanyan VS et al (2004) Synthesis of pyridazinone derivatives. *Chem Heterocycl Compd*. <https://doi.org/10.1023/B:COHC.0000046696.37815.62>
2. Özçelik AB, Özdemir Z, Sari S et al (2019) A new series of pyridazinone derivatives as cholinesterases inhibitors: Synthesis, in vitro activity and molecular modeling studies. *Pharmacol Reports* 71:1253–1263. <https://doi.org/10.1016/j.pharep.2019.07.006>
3. Benchat NE, Benalla A, El Kalai F et al (2008) Synthesis of 5-benzyl-2,6-dimethylpyridazin-3(2H)-one. *Molbank*. <https://doi.org/10.3390/M580>
4. Ramdani M, Benchat NE, Anafloos A, El Kalai F (2008) Microwave Synthesis of (4-hydroxy phenyl) 3-oxo butanoate. *Molbank*. <https://doi.org/10.3390/m561>
5. Mashuga ME, Olasunkanmi LO, Ebenso EE (2017) Experimental and theoretical investigation of the inhibitory effect of new pyridazine derivatives for the corrosion of mild steel in 1 M HCl. *J Mol Struct*. <https://doi.org/10.1016/j.molstruc.2017.02.002>
6. Asif M (2014) A Mini Review on Biological Activities of Pyridazinone Derivatives as Antiulcer, Antisecretory, antihistamine and Particularly Against Histamine H3R. *Mini-Reviews Med Chem*. <https://doi.org/10.2174/1389557514666141127143133>
7. Husain A, Ahmad A, Bhandari A, Ram V (2011) Synthesis and antitubercular activity of pyridazinone derivatives. *J Chil Chem Soc*. <https://doi.org/10.4067/S0717-97072011000300013>
8. Samuel K, Bose S (1987) Sites of action of pyridazinone herbicides (SANDOZ 9785 and 9789) on *Chlorella protothecoides*. *Proc Plant Sci* 97:415–423. <https://doi.org/10.1007/BF03053569>
9. Huang Q, Kong Y, Liu M et al (2008) Effect of oxadiazolyl 3(2H)-pyridazinone on the larval growth and digestive physiology of the armyworm. *Pseudaletia separata J Insect Sci*. <https://doi.org/10.1673/031.008.1901>
10. Chelfi T, Elaatioui A, Koudad M, et al (2015) Microwave synthesis of some substituted pyridazinones and their effect on the extraction efficiency of Pb(II) and Cd(II). *J Mater Environ Sci*
11. El Kalai F, Chelfi T, Benchat N et al (2019) New organic extractant based on pyridazinone scaffold compounds: Liquid-liquid extraction study and DFT calculations. *J Mol Struct*. <https://doi.org/10.1016/j.molstruc.2019.04.033>
12. Zarrouk A, Chelfi T, Dafali A, et al (2010) Comparative study of new pyridazine derivatives towards corrosion of copper in nitric acid: Part-1. *Int J Electrochem Sci*

13. El-Hajjaji F, Merimi I, Messali M, et al (2019) Experimental and quantum studies of newly synthesized pyridazinium derivatives on mild steel in hydrochloric acid medium. In: *Materials Today: Proceedings*. Elsevier Ltd, pp 822–831
14. El-Hajjaji F, Messali M, Martínez de Yuso MV et al (2019) Effect of 1-(3-phenoxypropyl) pyridazin-1-ium bromide on steel corrosion inhibition in acidic medium. *J Colloid Interface Sci* 541:418–424. <https://doi.org/10.1016/j.jcis.2019.01.113>
15. Chetouani A, Hammouti B, Aouniti A et al (2002) New synthesised pyridazine derivatives as effective inhibitors for the corrosion of pure iron in HCl medium. *Prog Org Coatings* 45:373–378. [https://doi.org/10.1016/S0300-9440\(02\)00123-6](https://doi.org/10.1016/S0300-9440(02)00123-6)
16. Khadiri A, Saddik R, Bekkouche K et al (2016) Gravimetric, electrochemical and quantum chemical studies of some pyridazine derivatives as corrosion inhibitors for mild steel in 1 M HCl solution. *J Taiwan Inst Chem Eng* 58:552–564. <https://doi.org/10.1016/j.jtice.2015.06.031>
17. Altunbaş Şahin E, Tezcan F, Solmaz R, Kardaş G (2020) Inhibitive effect of 4-amino-N-benzylidene-benzamide Schiff base on mild steel corrosion in HCl solution. *J Adhes Sci Technol* 34:135–152. <https://doi.org/10.1080/01694243.2019.1662202>
18. Chugh B, Singh AK, Chaoui A et al (2020) A comprehensive study about anti-corrosion behaviour of pyrazine carbohydrazide: Gravimetric, electrochemical, surface and theoretical study. *J Mol Liq*. <https://doi.org/10.1016/j.molliq.2019.112160>
19. Lgaz H, Chung IM, Salghi R et al (2019) On the understanding of the adsorption of Fenugreek gum on mild steel in an acidic medium: Insights from experimental and computational studies. *Appl Surf Sci*. <https://doi.org/10.1016/j.apsusc.2018.09.001>
20. Sayin K, Jafari H, mohsenifar F (2016) Effect of pyridyl on adsorption behavior and corrosion inhibition of aminotriazole. *J Taiwan Inst Chem Eng* 68:431–439. <https://doi.org/10.1016/j.jtice.2016.08.036>
21. Cisse MB, Zerga B, El Kalai F et al (2011) Two dipodal pyridin-pyrazol derivatives as efficient inhibitors of mild steel corrosion in HCL solution - Part I: Electrochemical study. *Surf. Rev, Lett*
22. Qiang Y, Li H, Lan X (2020) Self-assembling anchored film basing on two tetrazole derivatives for application to protect copper in sulfuric acid environment. *J Mater Sci Technol* 52:63–71. <https://doi.org/10.1016/j.jmst.2020.04.005>
23. Halambek J, Jukić M, Berković K, Vorkapić-Furač J (2012) Investigation of novel heterocyclic compounds as inhibitors of Al-3Mg alloy corrosion in hydrochloric acid solutions. *Int J Electrochem Sci*
24. Jafari H, mohsenifar Sayin FK (2016) Corrosion inhibition studies of N, N'-bis(4-formylphenol)-1,2-Diaminocyclohexane on steel in 1 HCl solution acid. *J Taiwan Inst Chem Eng* 64:314–324. <https://doi.org/10.1016/j.jtice.2016.04.021>
25. Rbaa M, Lakhri B (2019) Novel oxazole and imidazole based on 8-hydroxyquinoline as a corrosion inhibition of mild steel in HCl solution: Insights from experimental and computational studies. *Surfaces and Interfaces*. <https://doi.org/10.1016/j.surfin.2019.01.010>
26. Ouakki M, Galai M, Rbaa M et al (2019) Quantum chemical and experimental evaluation of the inhibitory action of two imidazole derivatives on mild steel corrosion in sulphuric acid medium. *Heliyon*. <https://doi.org/10.1016/j.heliyon.2019.e02759>
27. Salim R, Elaataoui A, Benchat N, et al (2017) Corrosion behavior of a smart inhibitor in hydrochloric Acid molar: Experimental and theoretical studies. *J Mater Environ Sci*
28. Ech-chihbi E, Nahlé A, Salim R et al (2019) An Investigation into Quantum Chemistry and Experimental Evaluation of Imidazopyridine Derivatives as Corrosion Inhibitors for C-Steel in Acidic Media. *J Bio- Tribo-Corrosion*. <https://doi.org/10.1007/s40735-019-0217-9>
29. Abd-El-Nabey BA, El-Housseiny G S, El-Naggar GA et al (2015) Inhibitive Action of Alhagi Maurorum Plant Extract on the Corrosion of Copper in 0.5 M H₂SO₄. *Phys Chem*. <https://doi.org/10.5923/j.pc.20150503.01>
30. Ech-chihbi E, Belghiti ME, Salim R et al (2017) Experimental and computational studies on the inhibition performance of the organic compound “2-phenylimidazo [1,2-a]pyrimidine-3-carbaldehyde” against the corrosion of carbon steel in 10 M HCl solution. *Surfaces and Interfaces*. <https://doi.org/10.1016/j.surfin.2017.09.012>
31. Rbaa M, Lgaz H, El Kacimi Y et al (2018) Synthesis, characterization and corrosion inhibition studies of novel 8-hydroxyquinoline derivatives on the acidic corrosion of mild steel: Experimental and computational studies. *Mater Discov*. <https://doi.org/10.1016/j.md.2018.11.003>
32. Ramya K, Mohan R, Anupama KK, Joseph A (2015) Electrochemical and theoretical studies on the synergistic interaction and corrosion inhibition of alkyl benzimidazoles and thiosemicarbazide pair on mild steel in hydrochloric acid. *Mater Chem Phys*. <https://doi.org/10.1016/j.matchemphys.2014.11.020>
33. Ramya K, Mohan R, Joseph A (2014) Adsorption and electrochemical studies on the synergistic interaction of alkyl benzimidazoles and ethylene thiourea pair on mild steel in hydrochloric acid. *J Taiwan Inst Chem Eng*. <https://doi.org/10.1016/j.jtice.2014.08.033>
34. Bentiss F, Mernari B, Traisnel M et al (2011) On the relationship between corrosion inhibiting effect and molecular structure of 2,5-bis(n-pyridyl)-1,3,4-thiadiazole derivatives in acidic media: Ac impedance and DFT studies. *Corros Sci*. <https://doi.org/10.1016/j.corsci.2010.09.063>
35. Singh AK, Quraishi MA (2010) The effect of some bis-thiadiazole derivatives on the corrosion of mild steel in hydrochloric acid. *Corros Sci*. <https://doi.org/10.1016/j.corsci.2010.01.007>
36. Zhang GA, Hou XM, Hou BS, Liu HF (2019) Benzimidazole derivatives as novel inhibitors for the corrosion of mild steel in acidic solution: Experimental and theoretical studies. *J Mol Liq*. <https://doi.org/10.1016/j.molliq.2019.01.060>
37. Sabet Bokati K, Dehghanian C (2018) Adsorption behavior of 1H-benzotriazole copper corrosion inhibitor on aluminum alloy 1050, mild steel and copper in artificial seawater. *J Environ Chem Eng*. <https://doi.org/10.1016/j.jece.2018.02.015>
38. Laabaissi T, Lgaz H, Oudda H, et al (2017) Comparative study of corrosion inhibition effect of benzodiazepine derivative on the carbon steel surface in 2.0 M H₃PO₄ and 1.0 M HCl mediums: Electrochemical, theoretical and Monte Carlo simulations studies. *J Mater Environ Sci*
39. Arjomandi J, Moghanni-Bavil-Olyaei H, Parvin MH et al (2018) Inhibition of corrosion of aluminum in alkaline solution by a novel azo-schiff base: Experiment and theory. *J Alloys Compd*. <https://doi.org/10.1016/j.jallcom.2018.02.288>
40. Kumari PDR, Nayak J, Shetty AN (2011) 3-Methyl-4-amino-5-mercapto-1,2,4-triazole as corrosion inhibitor for 6061 Al alloy in 0.5 M sodium hydroxide solution. *J Coatings Technol Res*. <https://doi.org/10.1007/s11998-011-9341-2>
41. Salim R, Ech Chihbi E, Oudda H, et al (2016) The inhibition effect of imidazopyridine derivatives on C38 steel in hydrochloric acid solution. *Der Pharma Chem*
42. Salhi A, Tighadouini S, El-Massaoudi M et al (2017) Keto-enol heterocycles as new compounds of corrosion inhibitors for carbon steel in 1 M HCl: Weight loss, electrochemical and quantum chemical investigation. *J Mol Liq*. <https://doi.org/10.1016/j.molliq.2017.10.040>
43. Galai M, Rbaa M, El Kacimi Y, et al (2017) Anti-corrosion properties of some triphenylimidazole substituted compounds in corrosion inhibition of carbon steel in 1.0 M hydrochloric acid solution. *Anal Bioanal Electrochem*

44. Su H, Liu Y, Gao X et al (2019) Corrosion inhibition of magnesium alloy in NaCl solution by ionic liquid: Synthesis, electrochemical and theoretical studies. *J Alloys Compd.* <https://doi.org/10.1016/j.jallcom.2019.03.318>
45. Ekanem UF, Umoren SA, Udousoro II, Udoh AP (2010) Inhibition of mild steel corrosion in HCl using pineapple leaves (*Ananas comosus* L) extract. *J Mater Sci.* <https://doi.org/10.1007/s10853-010-4617-y>
46. Yadav M, Kumar S, Kumari N, et al (2015) Experimental and theoretical studies on corrosion inhibition effect of synthesized benzothiazole derivatives on mild steel in 15% HCl solution. *Int J Electrochem Sci*
47. Elbakri M, Tourir R, Ebn Touhami M et al (2013) Inhibiting effects of benzamide derivatives on the corrosion of mild steel in hydrochloric acid solution. *Res Chem Intermed.* <https://doi.org/10.1007/s11164-012-0768-6>
48. Kharbach Y, Haoudi A, Skalli MK, et al (2015) The role of new phosphonate derivatives on the corrosion inhibition of mild steel in 1M H₂SO₄ media. *J Mater Environ Sci*
49. Elbelghiti M, Karzazi Y, Dafali A et al (2016) Experimental, quantum chemical and Monte Carlo simulation studies of 3,5-disubstituted-4-amino-1,2,4-triazoles as corrosion inhibitors on mild steel in acidic medium. *J Mol Liq.* <https://doi.org/10.1016/j.molliq.2016.01.076>
50. Fouda AS, Mohamed FS, El-Sherbeni MW (2016) Corrosion Inhibition of Aluminum-Silicon Alloy in Hydrochloric Acid Solutions Using Carbamidic Thioanhydride Derivatives. *J Bio- Tribo-Corrosion.* <https://doi.org/10.1007/s40735-016-0039-y>
51. Dao DQ, Hieu TD, Le Minh PT et al (2017) DFT study of the interactions between thiophene-based corrosion inhibitors and an Fe₄ cluster. *J Mol Model.* <https://doi.org/10.1007/s00894-017-3432-7>
52. Zarrouk A, Hammouti B, Dafali A et al (2014) A theoretical study on the inhibition efficiencies of some quinoxalines as corrosion inhibitors of copper in nitric acid. *J Saudi Chem Soc.* <https://doi.org/10.1016/j.jscs.2011.09.011>
53. Yadav M, Behera D, Kumar S, Sinha RR (2013) Experimental and quantum chemical studies on the corrosion inhibition performance of benzimidazole derivatives for mild steel in HCl. *Ind Eng Chem Res.* <https://doi.org/10.1021/ie400099q>
54. Ibeji CU, Ghosh D (2015) Singlet-triplet gaps in polyacenes: A delicate balance between dynamic and static correlations investigated by spin-flip methods. *Phys Chem Chem Phys.* <https://doi.org/10.1039/c5cp00214a>
55. Lukovits I, Kálmán E, Zucchi F (2001) Corrosion inhibitors - Correlation between electronic structure and efficiency. *Corrosion.* <https://doi.org/10.5006/1.3290328>
56. Pareek S, Jain D, Hussain S et al (2019) A new insight into corrosion inhibition mechanism of copper in aerated 3.5 wt.% NaCl solution by eco-friendly Imidazopyrimidine Dye: experimental and theoretical approach. *Chem Eng J.* <https://doi.org/10.1016/j.cej.2018.08.079>
57. Bendjeddou A (2016) Studies on chemical reactivity of *p*-aminophenyl benzene-fused bis tetrathiafulvalenes through quantum chemical approaches. *Am J Appl Chem.* <https://doi.org/10.1168/j.ajac.20160403.16>
58. Jmiai A, El Ibrahim B, Tara A et al (2018) Alginate biopolymer as green corrosion inhibitor for copper in 1 M hydrochloric acid: Experimental and theoretical approaches. *J Mol Struct.* <https://doi.org/10.1016/j.molstruc.2017.12.060>

Publisher's Note Springer Nature remains neutral with regard to jurisdictional claims in published maps and institutional affiliations.